
Proceedings Paper:
Hoang, K. orcid.org/0000-0001-7463-9681, Atallah, K., Odavic, M. et al. (2 more authors) (2019) Control development for hybrid vehicle powertrain with magnetic continuously variable transmission. In: 2018 IEEE International Conference on Electrical Systems for Aircraft, Railway, Ship Propulsion and Road Vehicles & International Transportation Electrification Conference (ESARS-ITEC). 2018 IEEE International Conference on Electrical Systems for Aircraft, Railway, Ship Propulsion and Road Vehicles & International Transportation Electrification Conference (ESARS-ITEC) , 07-09 Nov 2018, Nottingham, UK. IEEE . ISBN 978-1-5386-4192-7

https://doi.org/10.1109/ESARS-ITEC.2018.8607712

Control Development for Hybrid Vehicle Powertrain with Magnetic Continuously Variable Transmission

K D Hoang, K Atallah, and M Odavic
Department of Electronic and Electrical Engineering
The University of Sheffield
Sheffield, S1 4DE, United Kingdom
k.hoang@sheffield.ac.uk

J G Birchall and S Calverley
Magnomatics Limited
Park House, Bernard Road
Sheffield, S2 5BQ, United Kingdom
j.birchall@magnomatics.com

***Abstract*—This paper presents a control development for a hybrid vehicle powertrain with magnetic continuously variable transmission-MAGSPLIT. This is shown that in comparison with conventional continuously variable transmission (CVT) hybrid powertrain, a MAGSPLIT-based powertrain can provide similar functionality but with a number of advantages including efficiency improvement due to neglecting mechanical losses, inherent torsional vibration attenuation, and simplification of mechanical arrangement leading to improvement on powertrain safety and reliability. The proposed control strategy is developed with a MotoHawk hybrid transmission control unit (HTCU) and validated by both hardware in the loop (HIL) study and measurements from a MAGSPLIT-based powertrain brassboard.**

Keywords—CAN bus, dynamic control, HIL, hybrid vehicle, MAGSPLIT, mCVT, mode change, state machine.

I. INTRODUCTION

Recently, research into hybrid powertrain has seen substantial increased due to its advantages in reducing emissions and improving efficiency. To date, some hybrid powertrain topologies are matured and successfully commercialized [1]. Among them, the Hybrid Synergy Drive (HSD) [2] with a mechanical power-split device (PSD) together with two electrical machines (MG1 and MG2) allowing the internal combustion engine (ICE) to be independently operated along its maximum efficiency torque-speed curve during vehicle operation can be considered as one of the most popular hybrid powertrain concepts, Fig. 1(a). This functionality is considered to be similar as a continuously variable transmission (CVT) achieving via continuously controlling power flow and torque contributions from ICE, MG1, and MG2. Due to this advantage, hybrid vehicle with HSD-based powertrain is rated as one of the cleanest and most fuel efficient vehicle in the US in 2018 [3]. However, as power generation components of the HSD-based powertrain are rigidly connected via the PSD, mechanical-related issues such as PSD transmission failure, mechanical loss, and NVH (noise, vibration, and harshness) transmitted from ICE crankshaft via the PSD to the final drive (FD) are inevitable [4].

In [5]-[8], magnetic power split device concept named MAGSPLIT was presented, Fig. 1(b). Due to its magnetic coupling characteristic, a MAGSPLIT can provide similar combined functionalities of PSD and MG1 without mechanical issues. Thus, it results in the improvement of powertrain efficiency, NVH attenuation, and structural simplification

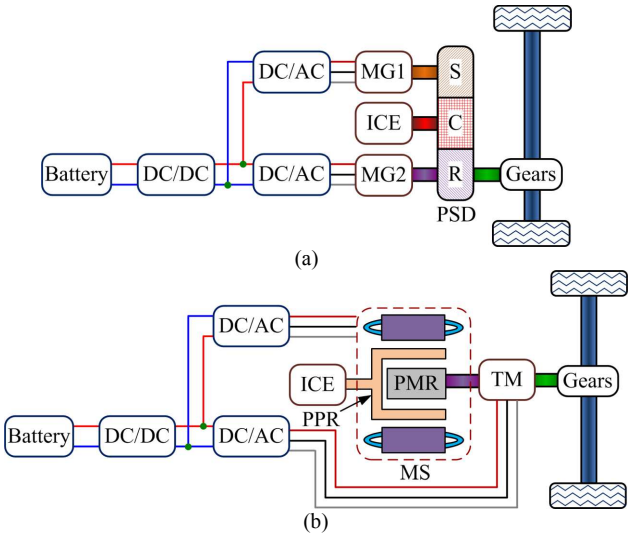

Fig. 1. CVT hybrid powertrain. (a) HSD-based concept [1]. (b) MAGSPLIT-based (mCVT) concept [5]-[8].

leading to improvement in powertrain safety and reliability. Steady state performance of MAGSPLIT-based hybrid powertrain was introduced in [9]. However, dynamic control scenarios such as mode change between hybrid and electric mode together with power flow determination which is highly essential for hybrid vehicle to maximize powertrain efficiency was not investigated. Preliminary control concepts for MAGSPLIT-based hybrid powertrain were introduced in [10] where appropriate bandwidth for engine speed controller and power distribution methodology were discussed.

In this paper, dynamic control development for a MAGSPLIT-based hybrid powertrain is presented and validated via both hardware in the loop (HIL) study and experimental measurements. First, the dynamic model for the studied MAGSPLIT-based hybrid powertrain is presented. Then, the proposed control method is introduced and implemented in a HIL system using a MotoHawk hybrid transmission control unit (HTCU) connecting via CAN bus with a dSPACE system acting as the MAGSPLIT-based hybrid powertrain. Results from the HIL system under different scenarios are presented to demonstrate the proposed control methodology and validate the functionality of the MAGSPLIT-based hybrid powertrain. For further demonstration, measurements from a MAGSPLIT-based hybrid powertrain test-rig are also introduced.

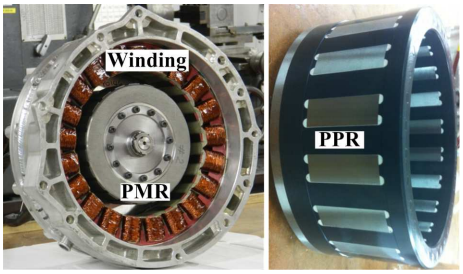

Fig. 2. MAGSPLIT structure illustration [8]. $n_{PPR} = 16$; $n_{PMR} = 7$; $n_{MS} = 9$.

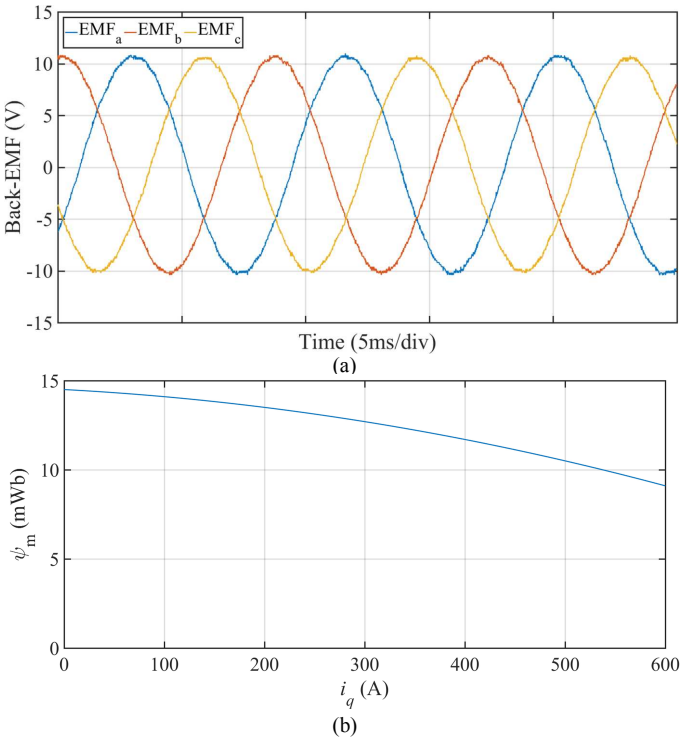

Fig. 3. Employed MAGSPLIT electrical characteristics. (a) Back-EMF. (b) PM flux linkage as a function of q-axis current.

II. MAGSPLIT-BASED HYBRID POWERTRAIN MODELLING

A. MAGSPLIT Modelling

As can be seen in Fig. 2, a MAGSPLIT includes a stator winding and two rotors: an inner PM rotor (PMR) and an outer pole piece rotor (PPR). Using magnetic gearing concepts [5]-[8], appropriate number of poles for rotating magnetic fields generated by the stator windings, the PMR and the number of pole-pieces on the PPR are selected. This arrangement enables the coupling between the stator winding and the two rotors [8].

1) MAGSPLIT Mechanical Model

In [5]-[8], MAGSPLIT operation has been described, and the steady-state relationships between speed, torque, and power of the PPR, the PMR, and the MAGSPLIT stator winding is as follows.

$$\omega_{PPR} n_{PPR} = \omega_{PMR} n_{PMR} + \omega_{MS} n_{MS} \quad (1)$$

$$\omega_{PPR} T_{PPR} + \omega_{PMR} T_{PMR} + \omega_{MS} T_{MS} = 0 \quad (2)$$

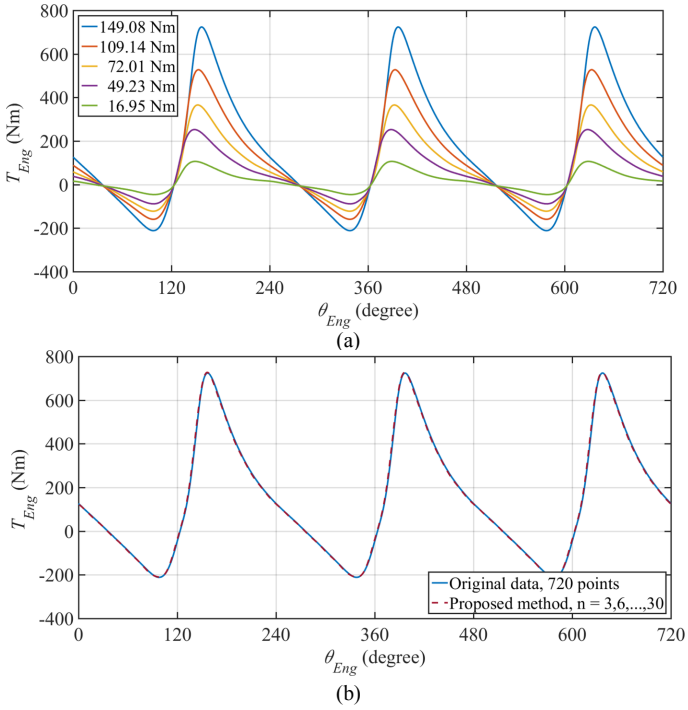

Fig. 4. Proposed method for ICE modelling. (a) Original torque data of employed ICE at 3000rpm (720 data points for each waveform). (b) Proposed model for ICE waveform-149.08Nm with 10 harmonics.

$$T_{MS}(n_{PPR} / n_{MS}) = T_{PMR}(n_{PPR} / n_{PMR}) = -T_{PPR} \quad (3)$$

where ω_{PPR}, ω_{PMR}, and ω_{MS} are the rotating speed of PPR, PMR, and the magnetic field generated by the stator winding, respectively; T_{PPR}, T_{PMR}, and T_{MS} are the torque of PPR, PMR, and stator winding, respectively; n_{PPR}, n_{PMR}, and n_{MS} are the number of pole-pieces on PPR, the number of pole pairs on PMR, and the number of pole pair of rotating stator magnetic field generated, respectively.

Using MAGSPLIT in Fig. 2, dynamic equation for PPR and PMR can be expressed in (4) where $J_{\Sigma PPR}$ and $J_{\Sigma PMR}$ are the total inertia of PPR and PMR, respectively; the superscript "load" denotes the outer load applied to the relevant rotor. In addition, balanced condition for the inner MAGSPLIT torque components is presented in (5).

$$\frac{d\omega_{PPR}}{dt} = \frac{1}{J_{\Sigma PPR}}(T_{PPR} + T_{PPR}^{load}); \quad \frac{d\omega_{PMR}}{dt} = +\frac{1}{J_{\Sigma PMR}}(T_{PMR} \quad T_{PMR}^{load}) \quad (4)$$

$$T_{PPR} + T_{PMR} + T_{MS} = T_{PPR}[1 - (n_{PMR} / n_{PPR}) - (n_{MS} / n_{PPR})] = 0 \quad (5)$$

2) MAGSPLIT Electrical Model

The MAGSPLT stator winding coupling with PPR and PMR can be modelled as a surface-mounted synchronous PM (SPM) machine [11], [12] for torque generation:

$$v_d = R_s i_d + \frac{d\psi_d}{dt} - \omega_{eMS}\psi_q; \quad v_q = R_s i_q + \frac{d\psi_q}{dt} + \omega_{eMS}\psi_d \quad (6)$$

$$\psi_d = L_s i_d + \psi_m; \quad \psi_q = L_s i_q \quad (7)$$

$$T_{MS} = (3/2) n_{MS} \psi_m i_q \quad (8)$$

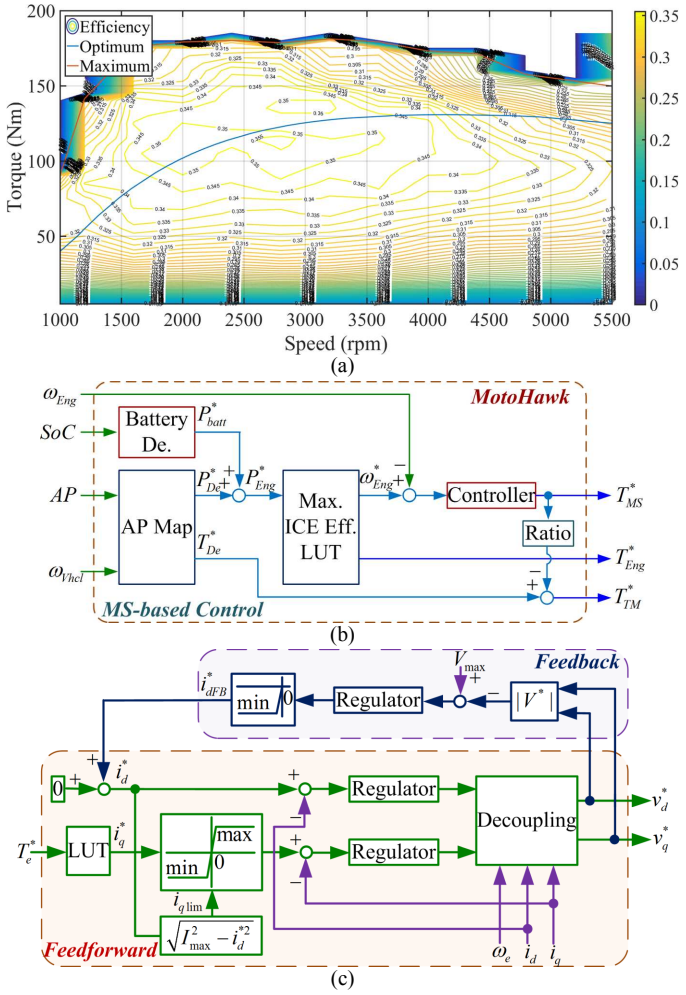

Fig. 5. Proposed hybrid control strategy. (a) ICE maximum efficiency curve. (b) Proposed hybrid control mode. (c) Control methodology for MAGSPLIT and traction machine.

where $v_{d,q}$, $i_{d,q}$, $\psi_{d,q}$, are the transformed (dq) voltages, currents, and stator flux-linkages, respectively; L_s is the stator synchronous inductance; ω_{eMS} is the stator electrical frequency; R_s is the stator resistance; ψ_m is the PM flux linkage associated with the space harmonic coupled to the stator winding. Measurements of the employed MAGSPLIT electrical parameters are presented in Fig. 3.

B. ICE Model

For simplicity, only instantaneous engine torque waveforms for different speed and torque values and engine flywheel inertia are considered for ICE modelling. Its inertia is combined with the PPR inertia. The instantaneous engine torque waveform varying as a function of crankshaft angular position is processed using Fourier analysis as shown in (9). As can be seen in Fig. 4, the proposed method can reduce the required data points for rebuilding a full given engine torque waveform at a specific speed from 720 data points into only 10 harmonics without compromising the original accuracy.

$$T_{Eng}(\theta_{Eng}) = T_{Eng(avg)} \sum_{n=1}^{\infty} [a_n \cos(n\theta_{Eng}) \quad b_n \sin(n\theta_{Eng})] \quad (9)$$

C. Traction Machine Model

A PM synchronous machine (YASA400) is selected for the MAGSPLIT-based hybrid powertrain. Its mathematical model is similar to that of MAGSPLIT electrical model in (6) to (8).

D. Battery Model

A battery model with open circuit voltage (V_{oc}) and state-of-charge (SoC) varying as a function of its demanded power presented in [12] is utilized for control development with a hardware in the loop (HIL) system. Details of the HIL system will be discussed in the next section.

E. Dynamic Tractive Load Model

The total tractive effort (F_{te}) and its components can be derived in (10) as below [12], [13].

$$F_{te} = F_{rr} + F_{ad} + F_{rg} + F_{la} \quad (10)$$

where $F_{rr} = \mu_{rr} m_v g \cos(\alpha)$; $F_{ad} = \rho_{air} C_d A_f v^2 / 2$

$F_{rg} = m_v g \sin(\alpha)$; $F_{la} = m_v a$

F_{rr}, F_{ad}, F_{rg}, and F_{la} is the rolling resistance force, aerodynamic force, road gradient force, and linear acceleration force, respectively; μ_{rr} is the rolling resistance coefficient; m_v is the vehicle mass; g is the gravitational acceleration; p_{air} is the air density; C_d is drag coefficient; A_f is the frontal area of the vehicle; v is the vehicle speed; and α is the road angle.

The total tractive effort in (10) must be balanced by the total torque generated from the MAGSPLIT-based hybrid powertrain transmitted to the final drive (FD).

$$T_{\Sigma} = r_{wheel} F_{te} \quad \eta_g n_g [T_{TM} \quad T_{MS}(n_{PMR} / n_{MS})] \quad T_{De} \quad (11)$$

where r_{wheel} is the wheel radius; n_g is the gear ratio of the final drive; η_g is the efficiency of the final drive; and T_{De} is the driver torque demand at the output of the final drive, respectively.

III. Proposed Control Strategy for MAGSPLIT-based Hybrid Powertrain

A. Hybrid Control Strategy

The control strategy for MAGSPLIT-based hybrid powertrain is developed for achieving of the driver torque demand at the wheels while the engine speed and torque is regulated for maximum efficiency, Fig. 5(a). As can be seen in Fig. 5(b), first, the accelerator pedal (AP) together with vehicle speed information (ω_{Vhcl}) is employed as the inputs of an AP map to generate driver power demand and relevant torque demand. On the other hand, based on instantaneous battery SoC information, power demand for charging/discharging battery pack, P_{batt}, is also obtained. Combination of the driver power demand and battery power demand results in engine power demand at the corresponding maximum efficiency. While engine torque demand is transmitted to engine control unit (ECU) using CAN bus, engine speed is maintained via MAGSPLIT torque on the PPR. This will also result in torque transmitted to the PMR, with the traction machine producing the remaining torque as shown in (11). This control strategy is named as MAGSPLIT-based control [10]. Torque control method for MAGSPLIT and traction machine including field

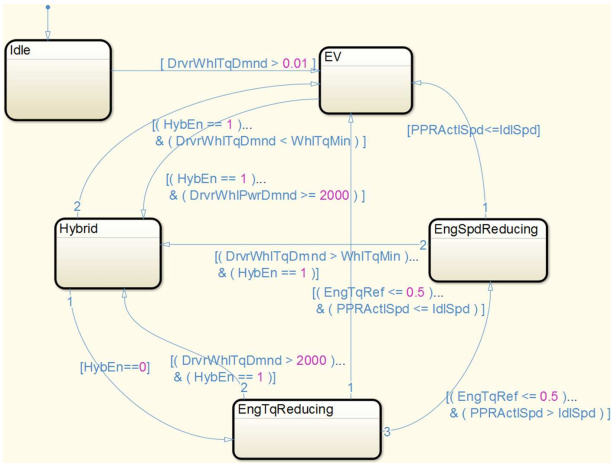

Fig. 6. Stateflow of mode change implementation for MAGSPLIT-based hybrid powertrain.

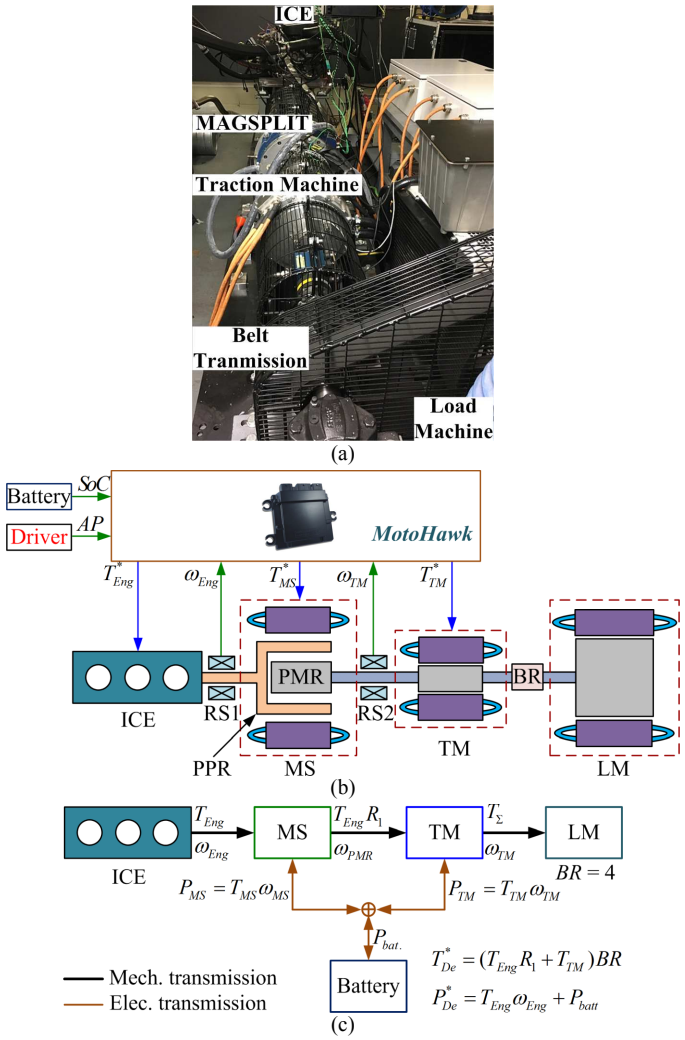

Fig. 7. Power transmission of MAGSPLIT-based hybrid powertrain. (a) Experimental test-rig. (b) HTCU with MotoHawk. (c) Power transmission.

weakening operation is illustrated in Fig. 5(c) and further details of the control methodology can be found in [11].

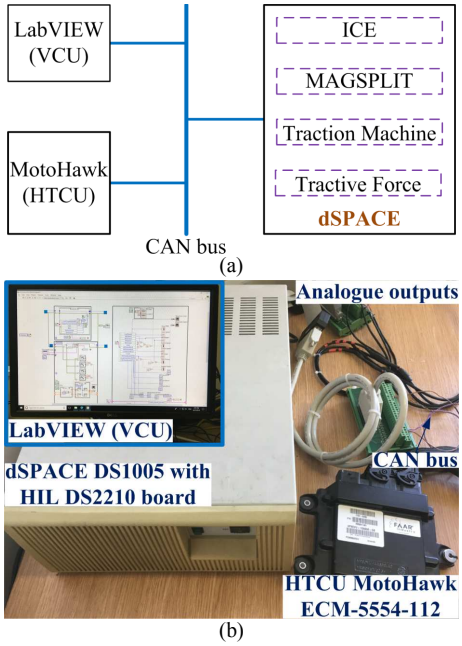

Fig. 8. HIL system for proposed control development. (a) Block diagram. (b). Implemenation system.

B. *Mode Change Strategy*

The Stateflow describing the proposed mode change implementation for the MAGSPLIT-based hybrid powertrain is illustrated in Fig. 6. When the tested powertrain is under hybrid mode, a changing operation mode requirement results in sequentially reducing the ICE torque demand then ICE speed demand while maintaining the driver torque demand at the wheels via regulating the traction machine torque demand. On the other hand, mode change from electric vehicle (EV) mode to hybrid mode will occur when demand on changing mode is requested by driver or controller and driver power demand is higher than the minimum ICE power limitation required for its optimum operation.

IV. Validation of Proposed Control Strategy with HIL Implementations and Measurments

The proposed control method is implemented for a MAGSPLIT-based hybrid test-rig shown in Fig. 7(a) including an ICE connected inline with a MAGSPLIT (MS) and a traction machine-TM (YASA400). A load machine (LM) acting as the vehicle tractive load is linked with the test-rig via a belt drive where belt ratio (BR) is as 4. Two resolvers (RS) are utilized to provide PPR and PMR speed information. A MotoHawk ECM-5554-112 is employed as a hybrid traction control unit (HTCU) and its input and output signals are shown in Fig. 7(b). The HTCU communicates with other device controllers via CAN bus. Power transmission through the hybrid powertrain is presented in Fig. 7(c). Further information of the employed MAGSPLIT can be found in [8].

In order to de-risk the control strategy, and avoid serious problems during testing of the real hybrid system in Fig. 7, the developed control strategy should be firstly implemented and validated in a HIL system [14]. Fig. 8 presents the developed

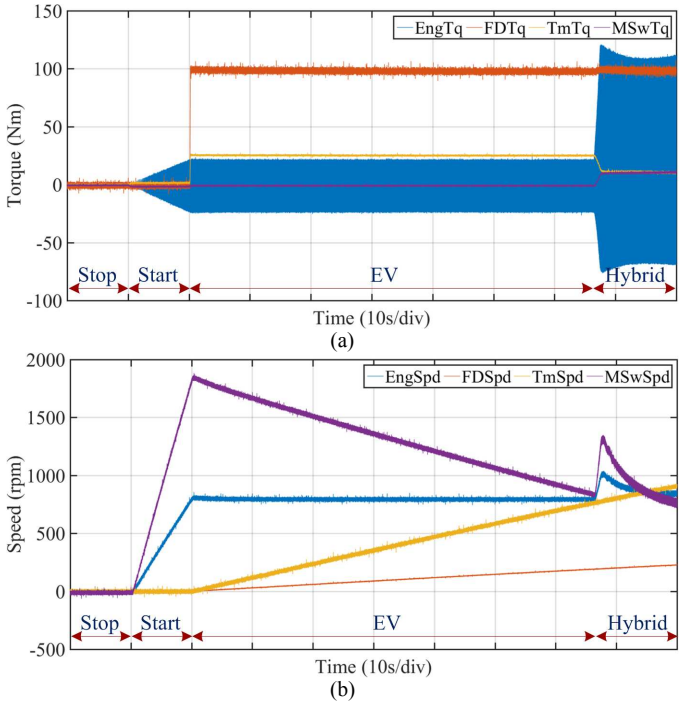

Fig. 9. Dynamic response of MAGSPLIT-based hybrid powertrain under start-up mode with 100Nm load demand. (a) Torque response. (b) Speed response.

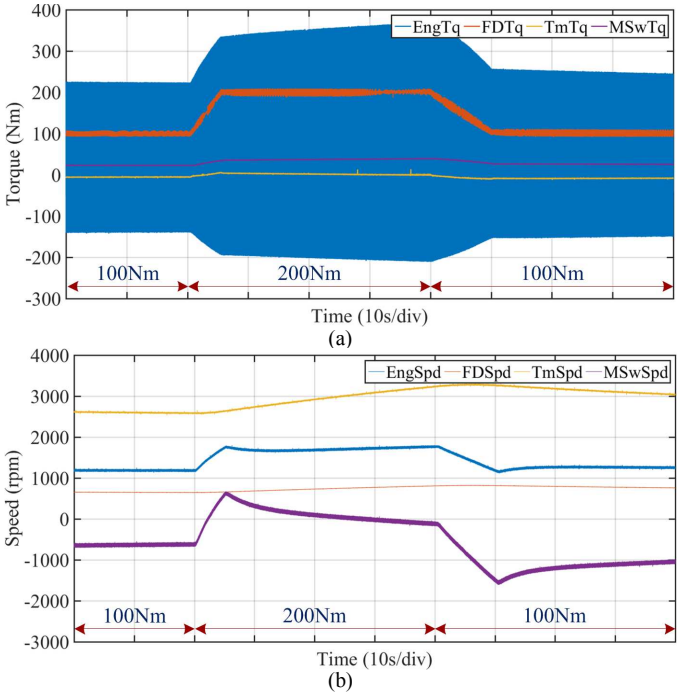

Fig. 10. Dynamic response of MAGSPLIT-based hybrid powertrain under step change on load demand from 100Nm to 200Nm. (a) Torque response. (b) Speed response.

HIL system for verifying the proposed control strategy under different scenarios. A dSPACE DS1005 with HIL DS2210 board is utilized to act as a test-rig dynamic system including ICE model, MAGSLPIT model, traction machine model, and tractive force model. A LabVIEW platform is employed as a driver and vehicle control unit (VCU) to give demand on load torque change and mode change. The proposed control strategy is developed in Matlab/Stateflow and realized on the HTCU. A CAN bus with baud-rate as 500kbps is utilized for communication between the dSPACE, HTCU, and VCU.

The start-up response of the MAGSPLIT-based hybrid powertrain under the HIL system is introduced in Fig. 9 where EngTq, FDTq, TmTq, and MSwTq is ICE, FD (wheel), traction machine, and MAGSPLIT torque, respectively; EngSpd, FDSpd, TmSpd, and MSwSpd is ICE, FD, traction machine, and MAGSPLIT speed. As can be seen in Fig. 9(b), the ICE speed is well regulated by the MAGSLIPT during acceleration and under load demand. On the other hand, Fig. 9(a) demonstrates the proposed hybrid control mode in Fig. 5(b) with the FD torque is well maintained at its demanded value (100Nm). It can be seen that while the ICE power is less than the threshold, the traction machine is delivering the required torque, however, as soon as the threshold is reached at about 95s, the ICE starts to produce power. Further validation for the proposed control method can be observed in Fig. 10 where the wheel torque follows the step change on demand. It is noted that the speed of the vehicle increases with increased wheel torque, Fig. 10(b).

Mode change between hybrid mode and EV mode is presented in Fig. 11. It is shown that the proposed control method can ensure a smooth transition between the hybrid mode and EV mode without adversely affecting vehicle speed, Fig. 11(b). In addition, all wheel torque waveforms in Figs. 9(a), 10(a), and 11(a) exhibit very low ripple compared to the ICE torque waveform, which demonstrates the inherent torque oscillation attenuation characteristic of the MAGSPLIT-based hybrid powertrain.

On the other hand, efficiency measurements of the tested MAGSPLIT obtained are shown in Fig. 12. As can be seen, for the tested MAGSPLIT to transmit full of its rated torque (180Nm) from its PPR to PMR under different PPR and PMR operation speeds, a maximum efficiency as 96% efficiency can be achieved resulting in improvement of total MAGSPLIT-based powertrain efficiency. Measurements of dynamic torque response from the hybrid test-rig (Fig. 7) are presented in Fig. 13 where the engine speed is regulated at 1200rpm by the MAGSPLIT. From t_1 to t_3, powertrain torque demand is set as zero with engine torque applying to the PPR is respectively as 10Nm for t_1, 20Nm for t_2, and 30Nm for t_3 resulting in relevant transmitted torques as 5.62Nm, 11.25Nm, and 16.87Nm at the MAGSPLIT output PMR. This measured results validates the transmitted gear ratio in (3) [8]. Based on (11), it is noted that the traction machine must balance the PMR torque to maintain a zero powertrain torque demand at the final drive. For timing t_4, t_5, and t_6, the powertrain torque demand is increased with 10Nm step. Since engine torque is still kept as 30Nm, a constant output MAGSPLIT torque at the PMR is achieved. Again, obtained final drive torque is maintained by both MAGSPLIT output torque and traction machine torque (11). The powertrain torque demand is reduced to zero for timing t_7. Then, engine torque demand is reduced to zero for timing t_8. The smooth torque response in Fig. 13 fully demonstrates the control development. In addition, the inherent torque oscillation attenuation characteristic of the MAGSPLIT-based

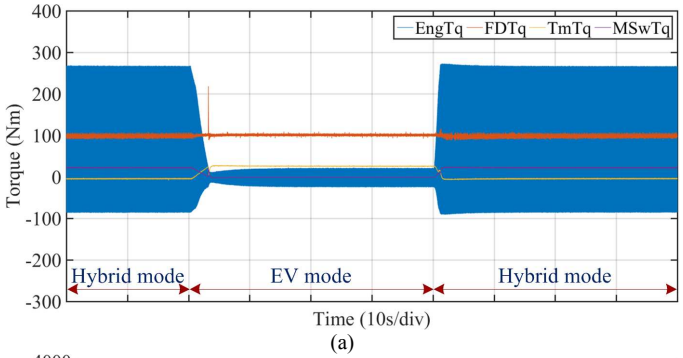

(a)

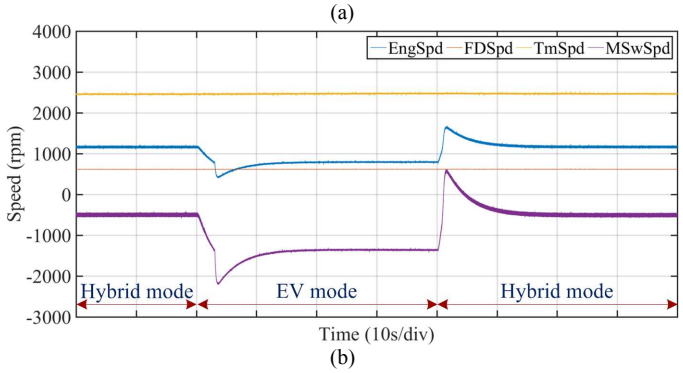

(b)

Fig. 11. Dynamic response of MAGSPLIT-based hybrid powertrain under mode change operation. (a) Torque response. (b) Speed response.

hybrid powertrain is highly illustrated in Fig. 13 with very low ripple for the MAGSPLIT output torque at its PMR.

V. Conclusions

In this paper, the development of a control strategy for a MAGSPLIT-based hybrid powertrain to achieve maximum ICE efficiency has been proposed and validated via HIL study and measurements from experimental test-rig. Under HIL implementation, it has been shown that a given ICE torque waveform can be represented by only 10 harmonics without compromising representation accuracy. This facilitates significantly HIL implementation for hybrid powertrain including ICE ripple representation.

It has been proven that a MAGSPLIT-based powertrain can provide similar functionality as HSD-based powertrain but with better performance including powertrain efficiency improvement, torsional vibration attenuation, and simplification of mechanical arrangement leading to improvement on powertrain safety and reliability.

References

[1] M. Ehsani, Y. Gao and J. M. Miller, “Hybrid electric vehicles: architecture and motor drives,” in *Proc. IEEE*, vol. 95, no. 4, pp. 719-728, April 2007.

[2] S. Sasaki, “Toyota 's newly developed hybrid powertrain,” *Power Semiconductor Devices and ICs, ISPSD 98.*, Kyoto, 1998, pp. 17-22.

[3] https://www.fueleconomy.gov/feg/pdfs/guides/FEG2018.pdf

[4] M. Komada, and T. Yoshioka, “Noise and vibration reduction technology in new generation hybrid vehicle development,” *SAE Technical Paper* 2005-01-2294, 2005.

[5] K. Atallah, J. Wang, S. D. Calverley and S. Duggan, “Design and operation of a magnetic continuously variable transmission,” *IEEE Trans. Ind. Appl.,* vol. 48, no. 4, pp. 1288 - 1295, Jul./Aug. 2012.

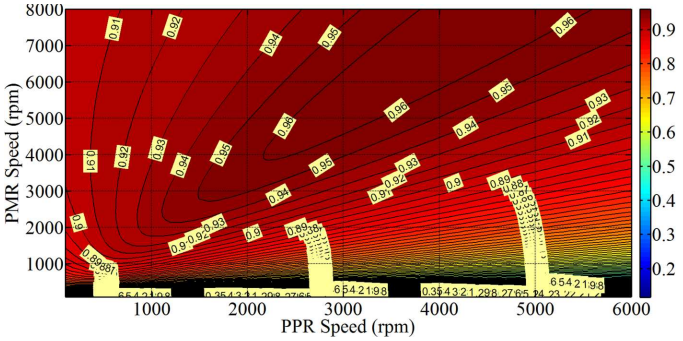

Fig. 12. MAGSPLIT efficiency measurements under different PMR and PPR operation speeds with full rated torque (180Nm) [8].

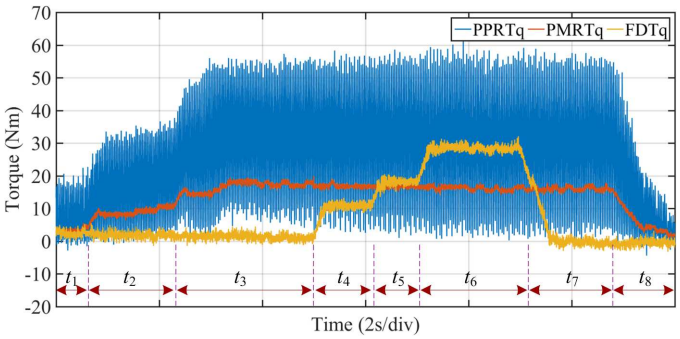

Fig. 13. Experimental dynamic torque response of MAGSPLIT-based hybrid powertrain.

[6] A. Zaini, N. Niguchi, K. Hirata, “Continously variable speed magnetic gear”, *The Japan Society Applied Electromagnetics and Mechanics*, vol. 20, no. 2, Mar. 2012.

[7] J. G. Birchall and S. D. Calverley, "Fast sizing method of a MAGSPLIT® power-split powertrain for use in hybrid electric vehicles," *6th Hybrid and Electric Vehicles Conference (HEVC 2016)*, London, UK, 2016, pp. 1-8.

[8] P. Chmelicek, S. Calverley, R. S. Dragan and K. Atallah, "Dual rotor magnetically geared power split device for hybrid electric vehicles," *2017 IEEE International Electric Machines and Drives Conference (IEMDC)*, Miami, FL, 2017, pp. 1-6.

[9] L. Sun, M. Cheng, H. Wen and L. Song, "Motion control and performance evaluation of a magnetic-geared dual-rotor motor in hybrid powertrain," in *IEEE Trans. Ind. Electron.*, vol. 64, no. 3, pp. 1863-1872, Mar. 2017.

[10] S. Calverley, G. Oshin, J. G. Birchall, K. Taylor, L. Rodrigues, D. Ooi, J. Akroyd, K. Atallah, K. Hoang, and A. Chapman, “Analysis, design and implementation of MAGSPLIT®; a novel dedicated hybrid transmission,” *6th CTI symposium 2017*, China, Sep. 25-27, 2017.

[11] K. D. Hoang and H. Aorith, “Online control of IPMSM drives for traction applications considering machine parameter and inverter nonlinearities,” *IEEE Trans. Transportation Electrification*, vol. 1, no. 4, pp. 312-325, Dec. 2015.

[12] K. D. Hoang and K. Atallah, “A rapid concept development technique for electric vehicle power trains,” *in Proc. IEEE Int. Conf. Connected Vehicles and Export (ICCVE) 2014*, Vienna, Austria, Nov. 3-7, 2014, pp. 191-198.

[13] K. D. Hoang and K. Atallah, “A rapid sizing concept of interior permanent magnet machine for traction applications”, *in Proc. IET Int. Conf. Power Electron. Mach., Drives (PEMD)* 2018, Liverpool, United Kingdom.

[14] H. Zhang, Y. Zhang and C. Yin, "Hardware-in-the-loop simulation of robust mode transition control for a series-parallel hybrid electric vehicle," in *IEEE Trans. Veh. Technol.*, vol. 65, no. 3, pp. 1059-1069, Mar. 2016.